

Kinetics and Mechanism of the Sonolytic Conversion of the Aqueous Perfluorinated Surfactants, Perfluorooctanoate (PFOA), and Perfluorooctane Sulfonate (PFOS) into Inorganic Products

Chad D. Vecitis, Hyunwoong Park, Jie Cheng, Brian T. Mader,[†] and Michael R. Hoffmann*

W. M. Keck Laboratories, California Institute of Technology, Pasadena, California 91125

Received: February 5, 2008

The perfluorinated surfactants perfluorooctane sulfonate (PFOS) and perfluorooctanoate (PFOA) are recognized as widespread in the environment as well as recalcitrant toward most conventional water treatment technologies. In this study, acoustic cavitation as driven by high-frequency ultrasound is shown to be effective in the degradation of aqueous solutions of PFOS and PFOA and effective over a wide range of concentrations from 10 nM to 10 μ M for a given compound. Sulfur, fluorine, and carbon mass balances indicate that mineralization occurs immediately following the degradation of the initial perfluorinated surfactant. Near complete conversion of PFOS and PFOA to CO, CO₂, F⁻, and SO₄²⁻ occurs due to pyrolytic reactions at the surface and vapor phase of transiently collapsing cavitation bubbles. The initial PFOS or PFOA pyrolytic degradation occurs at the bubble–water interface and involves the loss of the ionic functional group leading to the formation of the corresponding 1H-fluoroalkane or perfluoroolefin. The fluorochemical intermediates undergo a series of pyrolytic reactions in the bubble vapor leading to C₁ fluoro-radicals. Secondary vapor-phase bimolecular reactions coupled with concomitant hydrolysis converts the C₁ fluoro-radicals to carbon monoxide, carbon dioxide, and HF, forming a proton and fluoride upon dissolution. Sonochemical half-lives, which are calculated from high-temperature gas-phase kinetics, are consistent with kinetic observations and suggest that mineralization occurs shortly after initial perfluorinated surfactant interfacial pyrolysis.

Introduction

Over the last 60 years, fluorochemicals (FCs) have been used for a wide variety of applications such as water-proofing of materials, protective coating of metals, fire-fighting foams for electrical and grease fires, semiconductor etching, and in lubrication. The widespread use of these compounds is due to their favorable physical properties, which include chemical stability, low coefficients of friction, and low polarizabilities (i.e., fluorophilicity).¹ The same properties that make FCs valuable as commercial products make them difficult to treat using most conventional environmental remediation strategies or waste treatment technologies.^{2–4} For example, Schultz et al.³ reported that the total mass of PFOA and PFOS is not reduced (i.e., is resistant to physical and biological treatments) during conventional wastewater treatment processes. Consequently, fluorochemicals have become widespread in the environment.^{5–7}

Most conventional degradation technologies are ineffective for the in situ degradation of aqueous PFOS and PFOA, present in the aqueous phase, because they are inherently recalcitrant to chemical and microbiological treatment.^{2,3,8–11} Advanced oxidation processes (AOPs),¹² which utilize the hydroxyl radical, such as UV-ozonation,¹³ peroxone (i.e., a mixture of O₃ and H₂O₂),¹³ or Fenton's reagent (i.e., H₂O₂ and Fe²⁺ salts)^{13–15} have been shown to be ineffective for PFOA and PFOS destruction. A number of photolytic methods such as direct photolysis,^{15–20} persulfate photolysis,^{16,21–23} alkaline isopropanol photolysis,¹⁹ and photocatalysis^{15,24–28} have shown varying degrees of efficacy on higher concentrations of perfluorocarboxylates.

However, none of these methods lead to the mineralization of PFOS and PFOA. Reduction by elemental iron under near supercritical water conditions has been shown to be possible for PFOS degradation.²⁹ However, scale-up of high-pressure, high-temperature treatment systems is difficult.³⁰ Moriwaki et al.¹⁴ have shown that ultrasonic irradiation of aqueous solutions can degrade these compounds with fluoride and sulfate as the primary degradation products.

Sonochemistry, as induced by ultrasonic irradiation of aqueous solutions at near ambient temperatures and pressures, has been shown to be effective for the treatment of a wide variety of chemical contaminants.^{31–35} Ultrasonic pressure waves force the formation and quasi-adiabatic collapse of vapor bubbles formed from pre-existing gas nuclei.³⁶ The transient collapse of aqueous cavitation bubbles has been shown through chemical methods to raise average internal vapor temperatures near 4000 K^{37–39} and are supported by single-bubble collapse models,^{40–42} whereas bubble–water interface temperatures have been calculated to be in the range of 600 to 1000 K.³⁴ These transient high temperatures lead to in situ pyrolytic reactions in the vapor and interfacial regions of each collapsing bubble resulting in the breakdown of water producing hydroxyl radicals (OH), oxygen atoms (O), and hydrogen atoms (H). These transient radicals react readily with compounds in the bubble gas phase or at the bubble interface. Some of the radical species are dispersed into the bulk solution by nonspherical bubble collapse. Ultrasonic degradation is effective for the removal of contaminants with high Henry's Law constants^{43–45} that partition into the vapor phase of the bubble or for chemical contaminants that partition to the air–water interface^{46–48} such as PFOS and PFOA.¹⁴

* Corresponding author. E-mail: mrh@caltech.edu.

[†] Current address: 3M Environmental Laboratory, 3M Center, Building 260-05-N-17, Maplewood, MN 55144-1000.

We hereby report a detailed investigation into the kinetics and mechanism of the sonochemical conversion of aqueous PFOS and PFOA to inorganic constituents.

Experimental Methods

Ammonium perfluorooctanoate (APFO) and potassium perfluorooctanesulfonate (PFOS) standards consisting of a mixture of branched and linear isomers were provided by 3M. Ammonium acetate (>99%) and methanol (HR-GC > 99.99%) were obtained from EMD Chemicals Inc. Aqueous solutions were prepared with purified water using a Milli-Q system (18.2 M Ω cm⁻¹ resistivity).

Sonifications at frequencies of 354 and 618 kHz were performed using an Allied Signal Elac Nautik ultrasonic transducer (23.6 cm²) at an applied power of 150 W with the solution contained in a 600 mL jacketed glass reactor. The temperature was controlled with a Neslab RTE-111 refrigerated bath maintained at 10 °C. Sonifications performed at 500 kHz were completed with an Undatim ultrasonic transducer (25.5 cm²) at an applied power of 75 W with the solution contained in a 400 mL jacketed glass reactor. The temperature was controlled with a Haake A80 refrigerated bath set to 10 °C. All reactions were sparged with argon for at least 30 min prior to reaction. Initial solution pH was between 7 and 8 for all reactions. Calorimetry was done to determine the acoustic power transferred to solution. At 354, 500 and 618 kHz the applied (calorimetric) power densities in W L⁻¹ were 250 (200), 150 (128), and 250 (208), respectively. The applied acoustic power densities will be referred to in the text.

A number of reactor configurations, initial concentrations and mixtures were used for the various experiments. PFOS and PFOA were analyzed for in all experiments by an HPLC-MSD-Ion Trap (Agilent). Fluoride and sulfate analyses by ion chromatography (Dionex) were sonicated at 618 kHz, 250 W L⁻¹ and 6.4 W cm⁻² on a closed system where the produced gas was resparged into solution to retain all products: PFOS and PFOA were sonicated separately at initial concentrations of approximately 10 μ M. Trace gas analyses by GC-MS (Agilent) and FT-IR (Midac) were sonicated at 500 kHz, 150 W L⁻¹, and 2.9 W cm² on a closed system where the headspace was recirculated but not resparged through a 300 mL multiple reflection FT-IR cell with an in-line valved port for GC-MS sampling: PFOS and PFOA were sonicated simultaneously at a total initial concentration of 20 μ M (10 μ M each). The experiments where CO and CO₂ were measured during sonication were completed using 354 kHz, 250 W L⁻¹, and 6.4 W cm⁻² using a continuously sparged (100–125 mL min⁻¹) open system where the product gas was evacuated (\sim 100 mL min⁻¹) into a high-vacuum chamber through a stainless-steel membrane inlet to be analyzed by EI-MS (Balzers): PFOS and PFOA were sonicated separately at initial concentrations of 100 μ M. Reactor configurations and analytical procedures are detailed in the Supporting Information.

Results

Ultrasonic irradiation degradation kinetics of aqueous PFOS, [PFOS]_i = 200 nM, and PFOA, [PFOA]_i = 240 nM are plotted in Figure 1 (ν = 358 kHz, ρ_{PD} = 250 W L⁻¹, I_p = 6.4 W cm⁻²). The observed kinetics are quasi-exponential (i.e., the ln ([PFOX]_f/[PFOX]_i) vs time plot is linear) and is typical of what would be expected for PFOS and PFOA co-contamination in an environmental system where concentrations are in the picomolar to micromolar

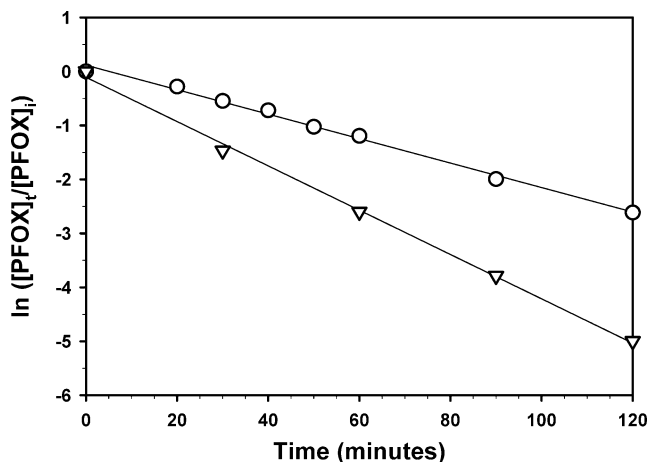


Figure 1. Pseudo-first-order plots of the degradation of PFOS and PFOA by ultrasonic irradiation at 354 kHz with a power density of 250 W L⁻¹ in the presence of Ar at 10 °C for [PFOS]_i = 200 nM and [PFOA]_i = 240 nM: PFOS (○) and PFOA (▽).

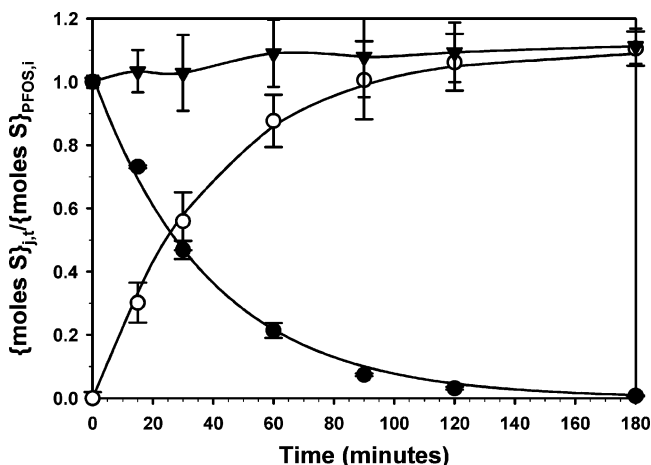


Figure 2. Normalized sulfur mass balance analyses vs time during the decomposition of PFOS by ultrasonic irradiation at 618 kHz at 250 W L⁻¹ under Ar at 10 °C where [PFOS]_i = 10 μ M. j = PFOS (●), sulfate (○) and sulfate + PFOS (▼).

range.⁷ Apparent pseudo-first-order kinetics are given in eq 1

$$\frac{d[\text{PFOX}]}{dt} = -k_{\text{app}}^{-\text{PFOX}}[\text{PFOX}] \quad (1)$$

where X = A or S and [PFOX] is the representative carboxylate or sulfonate concentrations and $k_{\text{app}}^{-\text{PFOX}}$ are the apparent first-order rate constants for each species. A linear fit of the kinetic plots gives $k_{\text{app}}^{-\text{PFOA}} = 0.041 \text{ min}^{-1}$ ($\tau_{1/2} = 16.9 \text{ min}$) and $k_{\text{app}}^{-\text{PFOS}} = 0.027 \text{ min}^{-1}$ ($\tau_{1/2} = 25.7 \text{ min}$). The PFOA degradation rate constant is 1.5 times that of PFOS. The observed pseudo-first-order kinetics are in agreement with results previously reported by Moriwaki et al.¹⁴ for the sonolytic degradation (200 kHz and 3 W cm⁻²) of aqueous PFOS and PFOA at 20 and 24 μ M, respectively. Similar sonochemical kinetics were also observed for hydrocarbon surfactants such as Triton X-100³² and linear alkyl benzyl sulfonates.⁴⁹

A time-dependent sulfur mass balance for an aqueous PFOS solution where [PFOS]_i = 10 μ M was obtained at ultrasonic conditions of 618 kHz, 250 W L⁻¹ and 6.4 W cm⁻². The PFOS sulfur mass balance is shown in Figure 2 in units of moles of sulfur per each species over total initial moles of PFOS sulfur. Aqueous sulfate ion, as detected by ion chromatography, was

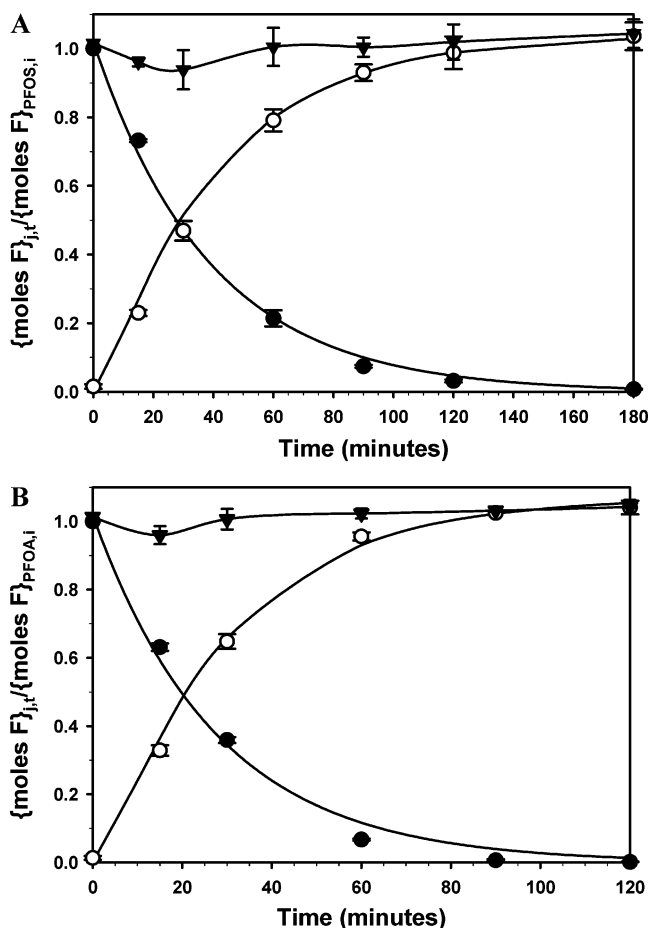


Figure 3. Normalized fluorine mass balance analyses vs time during the decomposition of PFOS and PFOA by ultrasonic irradiation at 618 kHz at 250 W L⁻¹ under Ar at 10 °C. (A) [PFOS]_i = 10 μM, *j* = PFOS (●), fluoride (○), and PFOS + Fluoride (▼). (B) [PFOA]_i = 12 μM, *j* = PFOA (●), fluoride (○), and PFOA + Fluoride (▼).

the only observed sulfur-containing product and has a formation half-life equivalent to the PFOS degradation half-life and thus is formed as PFOS is initially destroyed. At each point in time, the total sulfur balance, given by the sum of sulfate and PFOS sulfur, is equal to or greater than one.

The corresponding mass balance for fluorine of aqueous PFOS, [PFOS]_i = 10 μM, and PFOA, [PFOA]_i = 12 μM, during sonication for the same conditions is shown in Figure 3 in terms of moles of fluorine per species over total initial moles PFOX fluorine. In earlier work, Moriwaki et al. detected low levels of shorter-chain perfluoro-acids as reaction intermediates during the sonolytic degradation of PFOS and PFOA;¹⁴ however, we did not detect any of these intermediates during our experiments. Aqueous fluoride accounted for greater than 90% of the fluorine from the degraded PFOS and PFOA at any point in time during the reaction, as shown in panels a and b in Figure 3, respectively.

The solid lines through the PFOS, PFOA, sulfate, and fluoride data points shown in Figures 2 and 3 are obtained from kinetic analyses. For example, the PFOA fluorine mass balance data is fit using eq 2

$$\frac{\{\text{moles F}\}_{\text{PFOA},t}}{\{\text{moles F}\}_{\text{PFOA},i}} = \exp(-k_1^{-\text{PFOA}}t) \quad (2)$$

The fluoride and sulfate mass balance data are fit to a double exponential involving a single intermediate decay, (e.g., PFOS → I → F⁻ or SO₄²⁻). $k_1^{-\text{PFOX}}$ as determined from eq 2 is the

TABLE 1: Rate Constants for Time-Dependent PFOS and PFOA Sonochemical Sulfur and Fluorine Mass Balances

	$k_1^{-\text{PFOX}}$ (min ⁻¹) ^a	$k_2^{\text{F}^-}$ (min ⁻¹) ^b	$k_2^{\text{SO}_4^{2-}}$ (min ⁻¹) ^b
PFOS	0.026	0.3	>1.0
PFOA	0.036	0.3	

^a PFOX fluorine and sulfur sonochemical time dependence was fit to an exponential decay: $\exp(-k_1^{-\text{PFOX}}t)$. ^b Inorganic fluorine, fluoride, and sulfur, sulfate, sonochemical time-dependent growth was fit to exponential growth through a single decomposition intermediate: $(1/(k_1^{-\text{PFOX}} + k_2^{\text{X}^-}))(k_2^{\text{X}^-}(1 - \exp(-k_1^{-\text{PFOX}}t)) - k_1^{-\text{PFOX}}(1 - \exp(-k_2^{\text{X}^-}t)))$.

rate constant for the first decay, PFOS → I, and $k_2^{\text{X}^-}$ is the rate constant for the second decay, I → F⁻ or SO₄²⁻. For example, $k_2^{\text{SO}_4^{2-}}$ is determined through fitting the sulfate normalized mass balance data to eq 3

$$\frac{\{\text{moles S}\}_{\text{SO}_4^{2-},t}}{\{\text{moles S}\}_{\text{PFOS},i}} = \frac{1}{k_1^{-\text{PFOS}} + k_2^{\text{SO}_4^{2-}}} (k_2^{\text{SO}_4^{2-}}(1 - \exp(-k_1^{-\text{PFOS}}t)) - k_1^{-\text{PFOS}}(1 - \exp(-k_2^{\text{SO}_4^{2-}}t))) \quad (3)$$

The rate constants determined from the kinetic fits are given in Table 1. The PFOS and PFOA sonochemical decomposition rate constants decrease slightly at the somewhat higher initial concentrations used in the mass balance experiments as compared to those shown in Figure 1. The intermediate, I, conversion rate constant to sulfate, $k_2^{\text{SO}_4^{2-}}$, is >1 min⁻¹ and thus the sulfonate moiety (-CF₂-SO₃⁻) is converted quantitatively to sulfate (SO₄²⁻) shortly after the PFOS decomposition, -d[PFOS]/dt ≈ d[SO₄²⁻]/dt. This suggests that the sonolytic decomposition of PFOS proceeds via pyrolytic C-S bond cleavage⁵⁰ to yield an oxysulfur intermediate such as SO₃ or SO₃F⁻, which is readily hydrolyzed or oxidized to SO₄²⁻. A similar mechanism is expected for PFOA sonolysis where the initial bond cleavage occurs at the carbon-carbon bond between the carboxylate group and the fluorinated tail, (-CF₂-CO₂⁻), releasing CO₂.^{51,52} Initial ionic headgroup cleavage mechanism should produce a fluorinated alkane or alkene as the other primary sonolysis intermediate. These fluorochemicals are transformed to F⁻ at a rate constant of 0.3 min⁻¹ for both PFOS and PFOA, suggesting a similar fluoride production pathway for both species. The slower rate of fluoride production as compared to sulfate production during PFOS sonolysis is consistent with an initial C-S bond cleavage mechanism producing a fluorinated alkane intermediate that requires multiple, sequential pyrolytic steps prior to fluoride production.⁵³

The time-dependent sulfur and fluorine measurements are also consistent with the analysis of headspace gases by multiple reflection FT-IR and GC-MS during simultaneous sonication of PFOS and PFOA, [PFOS]_i = 10 μM and [PFOA]_i = 10 μM (500 kHz, 188 W L⁻¹ and 2.9 W cm⁻²). A large number of fluorinated gases were detected by GC-MS of the reactor headspace which was captured in an evacuated canister. The gases that were detected include (1) polyfluorinated alkanes, CHF₃, CH₂F₂, CH₃F, C₂F₅H, C₃F₇H, (2) polyfluorinated alkenes, C₂F₂H₂, C₂F₄, C₃F₆, C₄F₈, and (3) C₄-C₈ polyfluorinated alkenes. No sulfur-containing gases were detected. The most abundant of the fluorinated gas species were fluoroform and difluoromethane whose gas concentrations were monitored by online multiple reflection FT-IR (Figure 4: note the scale of

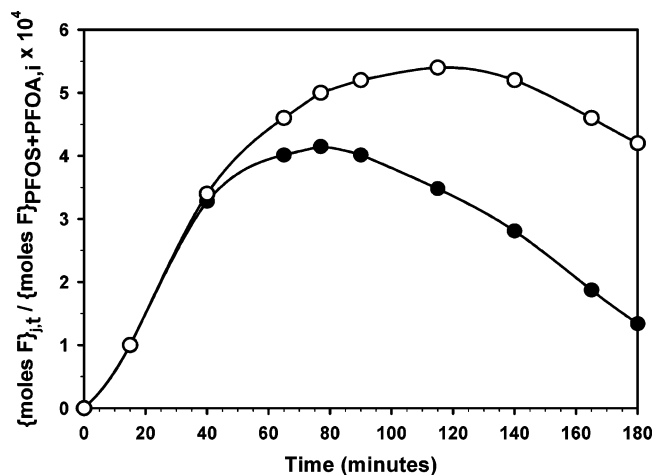


Figure 4. Normalized concentrations of the trace gases, CH_2F_2 and CHF_3 , vs time during the simultaneous decomposition of PFOS and PFOA by ultrasonic irradiation at 500 kHz at 188 W L^{-1} under Ar at 10°C , $[\text{PFOS}]_i = 10 \mu\text{M}$ and $[\text{PFOA}]_i = 12 \mu\text{M}$. $j = \text{CH}_2\text{F}_2$ (○) CHF_3 (●).

the y-axis is a factor of 1×10^4 lower than that of Figure 3 at all points in time). The maximum concentration of these two species amounted to $<0.1\%$ of the total fluorine during the simultaneous sonolysis of PFOS and PFOA. After these gas-phase products were formed, they were reentrained into the aqueous phase and destroyed by continued sonolysis. However, these species were not completely eliminated because the headspace was not resparged back into the reactor as the experiment was designed to accumulate any intermediate fluorochemicals for detection. Thus, passive gas transfer back into the sonicated solution was the limiting kinetic step of fluoroform and difluoromethane degradation. A table of all of the trace species detected by GC-MS after 120 min of sonolysis is listed in the Supporting Information: the total fluorine mole fraction of these species is 0.005 or less than 1%.

A carbon mass balance for the sonolytic degradation of PFOA and PFOS is plotted in panels a and b in Figure 5 as moles of carbon per species over the total initial moles of carbon versus time, $[\text{PFOS}]_i = 100 \mu\text{M}$ and $[\text{PFOA}]_i = 100 \mu\text{M}$ (354 kHz, 250 W L^{-1} , and 6.4 W cm^{-2}). The primary carbon containing species were the initial surfactant as detected by HPLC-MS and CO and CO_2 which were detected using real-time EI-MS. Other possible gaseous intermediates including formaldehyde, carbonyl fluoride, HF did not exceed the limit of detection. Real-time mass spectrometry was used to reduce the effect of any secondary gas product oxidation, $\text{CO}_{(\text{g})} \rightarrow \text{CO}_2_{(\text{g})}$, or reduction/thermolysis, $\text{CO}_2_{(\text{g})} \rightarrow \text{CO}_{(\text{g})}$,^{54,55} that may occur in subsequent bubble collapse events. After 120 min of sonolysis, $64.6 \pm 9.2\%$ of the carbon from decomposed PFOA was converted to CO and $32.1 \pm 7.0\%$ was converted to CO_2 , whereas in the case of PFOS sonolysis, the conversions to CO and CO_2 are $74.0 \pm$

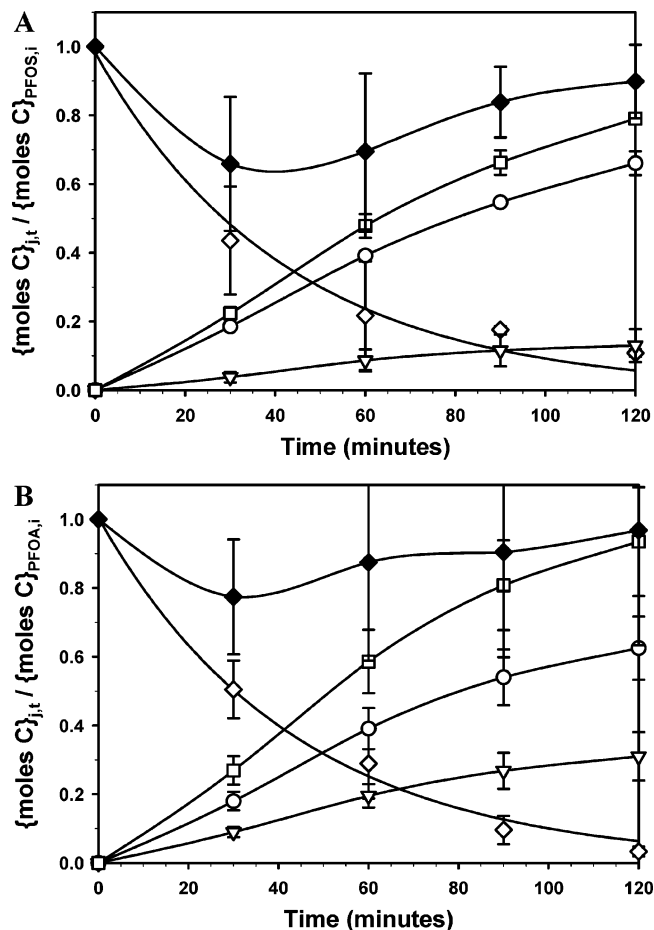


Figure 5. Normalized carbon mass balance plots vs time during the decomposition of PFOS and PFOA by ultrasonic irradiation at 354 kHz at 250 W L^{-1} under Ar at 10°C . (a) $[\text{PFOS}]_i = 100 \mu\text{M}$, $j = \text{PFOA}$ (◇), CO (○), CO_2 (▽), CO + CO_2 (□) and PFOS + CO + CO_2 (◆). (b) $[\text{PFOA}]_i = 100 \mu\text{M}$, $j = \text{PFOA}$ (◇), CO (○), CO_2 (▽), CO + CO_2 (□) and PFOA + CO + CO_2 (◆).

5.3% and $14.6 \pm 5.0\%$, respectively, yielding observed product ratios of $[\text{CO}]/[\text{CO}_2]_{\text{PFOA}} = 2.0$ and $[\text{CO}]/[\text{CO}_2]_{\text{PFOS}} = 5.1$.

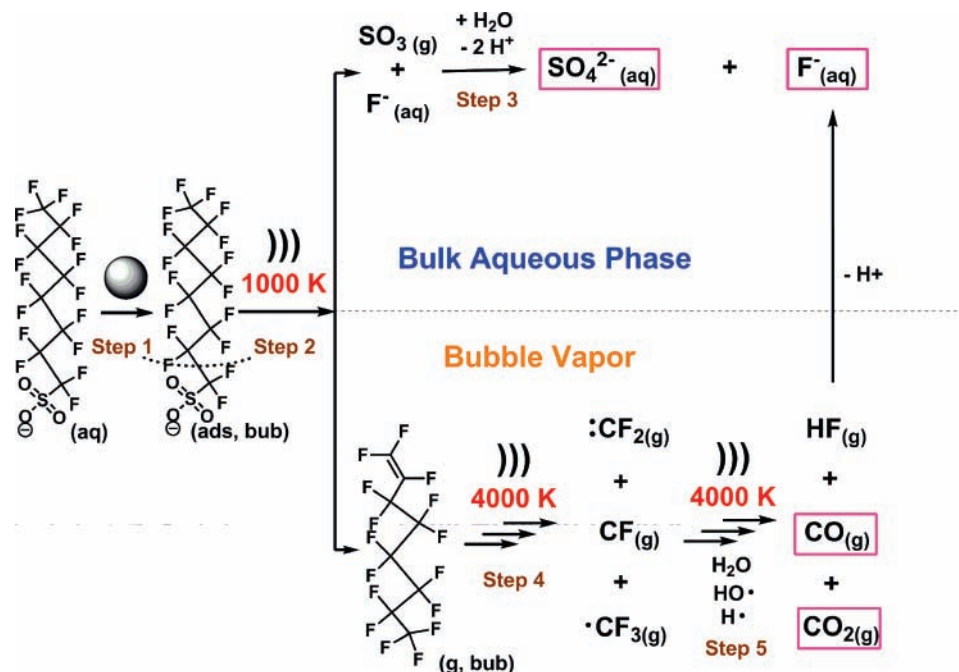
Discussion

Interfacial Pyrolysis of the Initial Perfluorinated Surfactant. PFOS and PFOA are surfactants.^{56–59} PFOS is considered to be a more effective surfactant since it has one more carbon than PFOA in its perfluorinated tail. Their surfactant properties coupled with their small Henry's constants (Table 2) precludes their diffusive transfer to the bubble vapor phase. These properties are consistent with sonochemical degradation at the bubble-water interface¹⁴ Oxidation by hydroxyl radicals^{32,47} at collapsing bubble–water interfaces is a possible mechanism. An upper limit for the second-order rate constant for the reaction

TABLE 2: Physicochemical Properties of the Initial Perfluorinated Surfactant and Primary Fluorochemical-Intermediates

	$C_{\text{w,sat}}^a$ (M) @ 20°C	p^b (atm) @ 20°C	K_{H} (atm M^{-1})	pKa	k_{OH}
PFOS- K^+	0.002	3.3×10^{-9}	N/A	-3.5	$<1 \times 10^6$ ^c
PFOA- NH_4^+	0.05 (gels)	9.2×10^{-8}	N/A	-0.5 ⁶⁷	$<1 \times 10^6$ ^c
PF-octene	1.4×10^{-8} ⁷⁴	0.03	2.1×10^6	n/a	2.4×10^{-12} ^d
1H-PF-octene	n/a	n/a	6.2×10^6	n/a	$10^{-9.2}e^{-63/RT}$ ^e
PF-heptene	1.4×10^{-7}	0.075	5.3×10^5	n/a	2.4×10^{-12} ^d
1H-PF-heptane	3.5×10^{-8} ⁷⁵	0.04	3.3×10^5	n/a	$10^{-9.2}e^{-63/RT}$ ^e

^a $C_{\text{w,sat}}$ estimation uses $N_{\text{H}_2\text{O}} = 1.28$, $\pi = 0.08$;⁷⁷ inserted refs are for experimental BPs. ^b Vapor pressures for the fluorochemical intermediates are estimated according to Mackay et al.⁷⁶ ^c Aqueous rates measured for hydroxyl plus TFA ($\text{M}^{-1} \text{s}^{-1}$).⁷⁸ ^d Gas-phase reaction of excess $\cdot\text{OH}$ + perfluoropropene at 295 K. ^e Gas-phase reaction of $\text{H}\cdot + \text{CF}_3\text{CHF}_2\text{CF}_3 - \text{H}\cdot$ abstraction ($\text{cm}^3 \text{ molecule}^{-1} \text{ s}^{-1}$).⁸⁰ ^f Calculated by the bond contribution method.⁸¹

SCHEME 1: Representative Scheme of the Sonochemical Degradation of PFOS and Transformation into Its Inorganic Constituents^a


^a Step 1: PFOS adsorption to the bubble–water interface. Step 2: Bubble–water interfacial pyrolytic decomposition of PFOS via cleavage of the C–S bond. Step 3: Hydrolysis of sulfur trioxide to sulfate. Step 4: Bubble vapor pyrolysis of the primary fluoro-intermediate into C₁ fluoro-radicals. Step 5: Transformation of C₁ fluoro-radicals within the bubble vapor to CO, CO₂, and HF, which is converted to a proton and a fluoride upon hydration. The inorganic products are highlighted in purple boxes.

of hydroxyl radical, $<1 \times 10^6 \text{ M}^{-1} \text{ s}^{-1}$, with both PFOA and PFOS has been estimated by analogy to the measured rate constant of hydroxyl radical reacting with trifluoroacetate. For comparison, oxalate ($\text{C}_2\text{O}_4^{2-}$), which is thought to be responsible for the slow TOC elimination during sonication,⁶⁰ has a second-order rate constant with hydroxyl radical of $4.7 \times 10^7 \text{ M}^{-1} \text{ s}^{-1}$, which is at least an order of magnitude greater than that of PFOS and PFOA. TOC elimination, and thus oxalate oxidation, has a sonolytic half-life under similar conditions of 10 h.⁶⁰ Given these arguments, hydroxyl radical oxidation appears to play a minor role in PFOS and PFOA degradation.¹⁴ Thus, interfacial pyrolytic decomposition appears to be the primary pathway for the sonochemical degradation of the perfluorinated surfactants.

Interfacial pyrolysis can be broken down conceptually into two fundamental steps. The first step involves the diffusion and adsorption of PFOS or PFOA to a transiently cavitating bubble interface (Step 1, Scheme 1) followed by a second step involving pyrolytic degradation at the cavitating-bubble interface (Step 2, Scheme 1).

The time-dependent mass balances shown in Figures 2–5 provide some insight into the sonolytic degradation mechanism of PFOS and PFOA. Of particular interest is the almost immediate production of inorganic sulfur (sulfate) and fluorine (fluoride) contrasted with a slightly delayed production of CO and CO₂. This suggests that

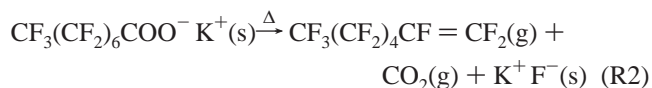
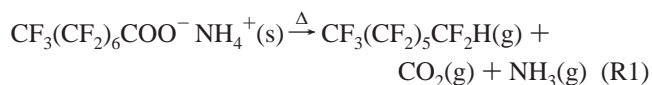
$$\frac{-d[\text{PFOX}]}{dt} = \frac{d(\text{mineralization})}{dt} \quad (4)$$

and that the primary intermediates produced during PFOS and PFOA decomposition appear to have much shorter half-lives than precursors. Given these observations, it is clear that

$$\frac{d[\text{PF-intermediate}]}{dt} \gg \frac{d[\text{PFOX}]}{dt} \quad (5)$$

and that the decomposition of the perfluoro-intermediates occurs in the vapor phase. Sonochemical reactions involving species that can partition to the vapor phase of a collapsing bubble (i.e., those having high Henry's constants) generally have the fastest degradation rates. The similarity between the fluorochemical surfactant degradation rates and the rates of mineralization, eq 4, suggests that the fluorointermediates formed from the initial pyrolytic reactions have high Henry's constants.

Pyrolysis of perfluorinated surfactants has been reported for several perfluoroalkancarboxylates and perfluoroalkanesulfonates in the solid phase^{50,52,61} and perfluoroalkancarboxylates in the vapor phase.^{51,62} The primary products of perfluoroalkancarboxylate pyrolysis product are reported to be the analogous 1H-perfluoroalkanes (R1) for NH_4^+ salts^{52,62} and perfluoroolefins (R2) with lesser amounts of perfluoroanhydrides and perfluoroacyl fluorides for alkaline and alkali salts.⁵²



Products generated during the thermal degradation of perfluorosulfonates have not been identified.⁵⁰ Ammonium perfluorooctanoate, which is thermally converted to the 1H-perfluoroalkane,^{52,62} decomposes at a temperature 50–100 K lower than that of the alkali and alkaline salts.^{50,52,61} Excess water has been observed to have an effect on the Arrhenius parameters of PFOA– NH_4^+ thermolysis⁶² by increasing log A values from 13.6 to 15.4 kJ mol^{-1} and activation energy from 150 to 172 kJ mol^{-1} . These activation energies are much lower than expected for the $-\text{CF}_2-\text{CF}_2-$ bond breaking, which are typically $>300 \text{ kJ mol}^{-1}$, Table 3. Initial cleavage of the C–C bond between

TABLE 3: Pyrolytic Kinetic Parameters for the Unimolecular Decomposition of Fluorochemicals^a

reaction	log A (s ⁻¹)	E _A (kJ mol ⁻¹)	k (T = 2500 K; s ⁻¹)	τ _{1/2} (ns)	ref
C ₃ F ₇ H → CF ₃ • + CF ₂ HCF ₂ •	16.9	372.6	1.29 × 10 ⁹	0.5	68
C ₃ F ₇ H → CHF ₂ • + CF ₃ CF ₂ •	16.6	372.6	6.47 × 10 ⁸	1.1	68
C ₃ F ₇ H → HF + C ₃ F ₆	13.9	280.5	1.29 × 10 ⁶	536.8	68
C ₄ F ₈ → CF ₃ • + C ₃ F ₅	16.1	292.9	9.48 × 10 ⁹	0.07	69
C ₄ F ₈ → C ₃ F ₆ + CF ₂	13.0	380.7	1.10 × 10 ⁵	6297.10	69
C ₄ F ₈ → C ₂ F ₄ + C ₂ F ₄	13.0	418.4	1.79 × 10 ⁴	38658.63	69
C ₆ F ₁₄ → C ₂ F ₅ • + C ₄ F ₉	17.2	330	2.00 × 10 ¹⁰	0.03	53
C ₆ F ₁₄ → 2 C ₃ F ₇ •	16.9	330	1.00 × 10 ¹⁰	0.07	53
C ₆ F ₁₄ → CF ₃ • + C ₅ F ₁₁ •	17.2	364	3.90 × 10 ⁹	0.18	53
C ₅ F ₁₁ • → C ₃ F ₇ • + C ₂ F ₄	13.6	168	1.22 × 10 ¹⁰	0.06	53
C ₄ F ₉ • → C ₂ F ₅ • + C ₂ F ₄	13.4	168	7.73 × 10 ⁹	0.09	53
C ₃ F ₇ • → CF ₃ • + C ₂ F ₄	13.3	186.4	2.53 × 10 ⁹	0.27	53
C ₃ F ₇ • → C ₂ F ₅ • + CF ₂ •	15.5	238.4	3.28 × 10 ¹⁰	0.02	53
C ₂ F ₅ • → CF ₃ • + CF ₂ •	15.6	235.4	4.78 × 10 ¹⁰	0.01	53
C ₂ F ₄ → 2 CF ₂ •	16.7	294	3.58 × 10 ¹⁰	0.02	53

^a $k = AT^b \exp(-E_A/RT)$, where E_A is in kJ mol⁻¹, $R = 0.00831$ kJ K⁻¹ mol⁻¹, and A and thus k are in s⁻¹; in all cases, $b = 0$.

the perfluorinated tail and the carboxylate group yields gaseous carbon dioxide and a perfluoroalkyl anion (R3). The perfluoroanion can form a 1H-perfluoroalkane by proton transfer (R4), which eliminates a C–F bond-breaking step (450 kJ mol⁻¹) and circumvents the perfluoroolefin formation pathway (R5).



A proton-transfer mechanism can explain the lower decomposition temperatures of the ammonium salts (R1) as compared to the alkali and alkaline salts (R2). Typical thermal decomposition of similar perfluoroalkane carboxylate and sulfonate salts⁵⁰ indicates that sulfonate salts decompose at higher temperatures (e.g., 100–200 K higher) than corresponding carboxylate salts. These observations are consistent with the relative sonolytic degradation rates of PFOA ($k_{\text{app}}^{\text{-PFOA}} = 0.041$ min⁻¹) and PFOS ($k_{\text{app}}^{\text{-PFOS}} = 0.027$ min⁻¹) in spite of the greater interfacial activity and tendencies of PFOS.

In summary, initial PFOX decomposition involves the loss of the ionic headgroup: CO₂ in the case of PFOA (R1) and SO₃ in the case of PFOS. The pyrolytic cleavage of the ionic headgroups of both molecules leads to the formation of C₇ and C₈ perfluorocarbanion intermediates for PFOA and PFOS, respectively. The perfluorocarbanion is protonated to form a 1H-perfluoroalkane (R4) or undergoes fluoride elimination to form a perfluoroolefin (R5) (Step 2, Scheme 1). SO₃ produced during PFOS decomposition hydrolyzes rapidly (Step 3, Scheme 1) to form sulfate with the release of two protons.

Unimolecular Decomposition of the Fluorocarbon Tail.

The organo-fluorines in the C₇ and C₈ fluorochemical intermediates are sonochemically converted into F⁻ with a pseudo first-order rate constant of 0.3 min⁻¹ (τ_{1/2} = 2.3 min). The fluorochemical intermediate degradation rates are greater than the sonochemical degradation rates reported for chlorinated hydrocarbons.^{63,64} The Henry's constants for the likely 1H-perfluoroalkane (R4) and perfluoroolefin (R5) intermediates have been estimated by two different methods and determined to be on the order of 10⁵ to 10⁶ atm L mol⁻¹ (Table 1). Colussi et al.⁴⁵ established a correlation between the Henry's constant, K_{H}^x , for chlorinated hydrocarbons, x , and their apparent sonolytic degradation rate constants where: $k_{\text{sono,app}}^{-x} = 4.5 \times$

10⁻³ $K_{\text{H}}^{x,0.3}$ (s⁻¹). Given the range of Henry's constants for the perfluoro-intermediates, we estimate sonolytic half-lives from 1 to 3 s; these times are shorter but consistent with the observed fluoride production kinetics (τ_{1/2} = 140 s). Partitioning of fluorocarbons between phases cannot be estimated accurately using parameters determined for hydrocarbons.^{65–67} For example, measurement⁶⁶ of Henry's constants for perfluoroolefins is difficult. The perfluoro-intermediates may not immediately partition into the vapor-phase rapidly, but dwell for a period of time at the bubble-water interface before vapor-phase pyrolytic decomposition.

The apparent discrepancy between the observed F⁻ production rates and estimated degradation rates of these fluoro-intermediates may be due to a greater number of acoustic cycles to produce F⁻, CO, and CO₂. The unimolecular decomposition kinetics for C₇ and C₈ fluorocarbon-intermediates in question have not been determined experimentally or computationally. Instead, we will use kinetic parameters for shorter-chain fluorochemicals in order to estimate decomposition rates.

The pyrolytic kinetics of the experimental technique is listed in parentheses for 1H-perfluoropropane (IRMPD),⁶⁸ 1-perfluorobutene (IRMPD),⁶⁹ perfluorohexane (VLPP),⁵³ and their decomposition intermediates are listed in Table 3. First-order rate constants and half-lives are estimated using a temperature of 2500 K, which is less than the average vapor temperature achieved during a single transient cavitation event^{37,39,70,71} in water. At 2500 K, experimentally determined Arrhenius parameters should be valid. It is noted that all of the possible fluorocarbon-intermediates have at least one estimated C–C bond breaking decomposition pathway with a half-life under 100 ps and the subsequent fluoroalkyl radical intermediates all have faster C–C bond-breaking kinetics. The unimolecular decomposition kinetics will dominate the bimolecular reaction kinetics and we can assume that the initial fluoro-intermediate will dissociate into C₁ fluoro-radical constituents prior to any intervening bimolecular reactions.

In Scheme 2, we propose a degradation mechanism for perfluoroctene in a cavitating bubble. The values above the reaction arrows are the estimated times for greater than 99% of the reaction. The stoichiometries for 1H-perfluoroheptane and perfluoroctene decompositions are given in reactions 6 and 7, respectively

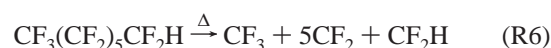


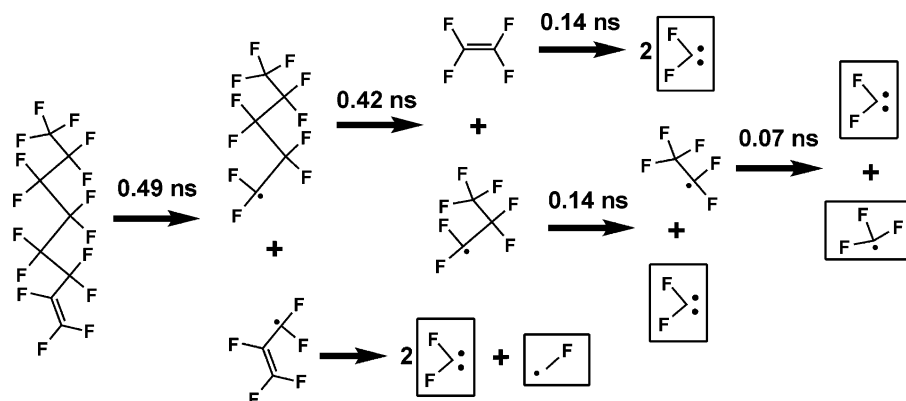
TABLE 4: Pyrolytic Kinetic Parameters for Bimolecular Reactions of C₁-Fluoro-Radicals

reaction	A (molecule cm ⁻³ s ⁻¹)	b	E _A (kJ mol ⁻¹)	k (T = 4000 K; molecule cm ⁻³ s ⁻¹)
CHF ₂ • + H → CH ₂ F ₂	2.75 × 10 ⁶	-0.32	32.2	1.22 × 10 ⁻¹⁹
CHF ₂ • + H → CHF: + HF	1.50 × 10 ¹⁴	-0.11	0.5	9.85 × 10 ⁻¹¹
CHF ₂ • + H → CF ₂ : + H ₂	5.50 × 10 ³	2.41	0	4.38 × 10 ⁻¹²
CHF ₂ • + OH → CHF:O + HF	2.40 × 10 ¹³	0	0	3.99 × 10 ⁻¹¹
CHF ₂ • + O → CF ₂ :O + H	3.70 × 10 ¹³	0	0	6.14 × 10 ⁻¹¹
CF ₃ • + H → CF ₂ : + HF	5.50 × 10 ¹³	0	0	9.13 × 10 ⁻¹¹
CF ₃ • + OH → CF ₂ :O + HF	2.00 × 10 ¹³	0	0	3.32 × 10 ⁻¹¹
CF ₃ • + O → CF ₂ :O + F	1.90 × 10 ¹³	0	0	3.16 × 10 ⁻¹¹
CF ₂ : + H ₂ O → CHF:O + HF	5.00 × 10 ¹²	0	104.6	3.57 × 10 ⁻¹³
CF ₂ : + OH → CF:O + HF	4.00 × 10 ¹²	0	14.6	4.28 × 10 ⁻¹²
CF ₂ : + OH → CF ₂ :O + H	2.00 × 10 ¹³	0	14.6	2.14 × 10 ⁻¹¹
CF ₂ : + H → CF + HF	2.00 × 10 ¹⁴	0	14.6	2.14 × 10 ⁻¹⁰
CF ₂ : + O → CF:O + F	7.00 × 10 ¹³	0	4.2	1.02 × 10 ⁻¹⁰
CF + H ₂ O → CHF:O + H	2.00 × 10 ¹³	0	71.1	3.91 × 10 ⁻¹²
CF + OH → CO + HF	4.00 × 10 ¹³	0	4.2	5.85 × 10 ⁻¹¹
CF + H → CH + F	4.00 × 10 ¹³	0	2.8	6.11 × 10 ⁻¹¹
CF + O → CO + F	4.00 × 10 ¹³	0	4.2	5.85 × 10 ⁻¹¹
CHF: + H ₂ O → CH ₂ O + HF	5.00 × 10 ¹²	0	27.2	3.66 × 10 ⁻¹²
CHF: + OH → CHO + HF	4.00 × 10 ¹²	0	0	6.64 × 10 ⁻¹²
CHF: + OH → CFH:O + H	2.00 × 10 ¹³	0	0	3.32 × 10 ⁻¹¹
CHF: + H → CH + HF	3.00 × 10 ¹⁴	0	0	4.98 × 10 ⁻¹⁰
CHF: + O → CO + HF	9.00 × 10 ¹²	0	12.9	1.01 × 10 ⁻¹¹
CHF:O + M → CO + HF	2.50 × 10 ²⁵	-3	179.8	2.90 × 10 ⁻¹²
CHF:O + H → CF:O + H ₂	1.10 × 10 ⁸	1.77	12.5	2.98 × 10 ⁻¹⁰
CHF:O + OH → CF:O + H ₂ O	1.70 × 10 ⁹	1.18	0	5.03 × 10 ⁻¹¹
CHF:O + O → CF:O + OH	9.00 × 10 ¹²	0	12.9	1.01 × 10 ⁻¹¹
CF ₂ :O + H ₂ O → CO ₂ + 2 HF	7.40 × 10 ³	3.84	105	3.54 × 10 ⁻¹⁴
CF ₂ :O + H → CF:O + HF	1.20 × 10 ¹⁰	0.83	93.3	1.18 × 10 ⁻¹²
CF ₂ :O + OH → CO ₂ + HF + F	2.70 × 10 ³	2.38	87.8	1.20 × 10 ⁻¹³
CF:O + H → CO + HF	1.20 × 10 ¹⁴	0	0	1.99 × 10 ⁻¹⁰
CF:O + OH → CO ₂ + HF	3.00 × 10 ¹³	0	0	4.98 × 10 ⁻¹¹
CF:O + O → CO ₂ + F	3.00 × 10 ¹³	0	0	4.98 × 10 ⁻¹¹
F + H ₂ O → HF + OH	1.30 × 10 ⁹	1.5	0	5.46 × 10 ⁻¹⁰
F + H ₂ → HF + H	2.60 × 10 ¹²	0.5	0	2.73 × 10 ⁻¹⁰
F + OH → HF + O	2.00 × 10 ¹³	0	0	3.32 × 10 ⁻¹¹

The C₁ fluoro-radical products retain their original C–F bond intact since the average C–C– bond strength (410 kJ mol⁻¹) is substantially less than the average C–F bond strength (530 kJ mol⁻¹). For comparison, the O–H bond strength of water is 498 kJ mol⁻¹.

Numerical simulations by Yasui et al.⁴² and Colussi et al.⁴⁰ have modeled the time-dependent temperature evolution and the subsequent chemical reactions taking place during a transiently cavitation event at 300 kHz. In both cases, the maximum bubble-vapor temperatures were above 2500 K. Under these conditions, the characteristic time for the reactions portrayed in Scheme 2 to take place is 1 ns. Therefore, the C₇ or C₈ fluoro-intermediates should be completely dissociated into C₁ fluoro-radical constituents in a single acoustic cycle.

Transformation of C₁ Fluoro-Radical Intermediates into CO and CO₂. The initial sonochemical decomposition steps of PFOS and PFOA produce either C₇ or C₈ 1H-perfluoroalkanes (R4) or perfluoroolefins (R5) (Step 2, Scheme 1). These intermediates are then pyrolytically decomposed into C₁ fluoro-radicals (R6, R7): trifluoromethyl radical (•CF₃), difluoromethyl radical (•CHF₂), fluoromethylidyne (CF), and difluorocarbene (:CF₂) (Step 4, Scheme 1). The C₁ fluoro-radicals are subsequently transformed into carbon monoxide and carbon dioxide. A series of bimolecular reactions with H₂O, H•, HO•, and O-atom are proposed in Table 4 for the conversion of the C₁ fluoro-radicals into CO, CO₂ and HF.⁷² The second-order reaction rate constants are estimated at 4000 K, where H₂O thermolysis is significant. Several assumptions are made when

SCHEME 2: Representative Scheme of a Fluoro-Intermediate Unimolecular Decomposition Mechanism Yielding C₁ Fluoro-Radicals (Step 4, Scheme 1)^a

^a The time for >99% reaction progress at 2500 K is reported above the reaction arrow. The C₁ fluoro-radicals are shown in boxes.

TABLE 5: Estimated CO/CO₂ Product Ratios for PFOS and PFOA Sonolysis under Various Bubble Vapor Chemical Compositions

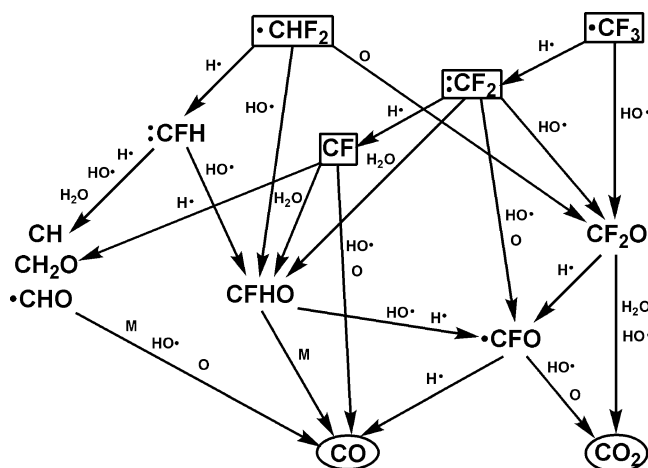
	case I			case II			case III		
water vapor %	10.0	1.0	0.1	10.0	1.0	0.1	10.0	1.0	0.1
radical %	1.0	1.0	1.0	0.1	0.1	0.1	Range	Range	Range
CFO CO/CO ₂	2.00	2.00	2.00	2.00	2.00	2.00	0.40	0.40	0.40
CF ₂ O CO/CO ₂	0.90	1.43	1.52	0.19	0.90	1.43	0.06	0.14	0.16
CHF CO/CO ₂	94.73	89.33	88.79	750.99	479.89	452.78	23.53	17.13	16.49
CHFO CO/CO ₂	4.43	4.43	4.43	26.32	26.32	26.32	5.45	5.45	5.45
PFOS CO/CO ₂	5.21	6.66	6.87	4.63	5.99	6.79	1.05	1.21	1.25
PFOS calcd/expt	1.02	1.31	1.35	0.91	1.17	1.33	0.21	0.24	0.25
PFOA CO/CO ₂	2.48	2.85	2.90	2.20	2.69	2.94	0.78	0.86	0.89
PFOA calcd/expt	1.24	1.43	1.45	1.10	1.35	1.47	0.39	0.43	0.44

estimating the high-temperature kinetics. First, it is assumed that the radical intermediates constitute a negligible fraction of the total bubble vapor content; as a consequence fluoro-radical/fluoro-radical reactions can be neglected. Second, the C₁ fluoro-radical unimolecular decomposition is assumed to be of minor importance, since at aqueous cavitation temperatures,^{39,70} the thermolytic splitting of water, which has a lesser bond strength than fluoro-radical C–F bonds, is dominant. Finally, the sonolytic interconversion of CO and CO₂^{48,54} is assumed to be insignificant since CO₂ $\xrightarrow{H\cdot}$ CO has a half-life on the order of 1 h under similar conditions.⁵⁴ Furthermore, if interconversion of CO and CO₂ were significant during sonolysis, then the CO/CO₂ product ratios for PFOS and PFOA would be similar; however, we observe [CO]/[CO₂]_{PFOA} = 2.0 and [CO]/[CO₂]_{PFOS} = 5.1.

The branching ratios for the pyrolytic transformations of the C₁ fluoro-radicals can be calculated using relative H₂O, H \cdot , HO \cdot , and O-atom vapor concentrations estimated from numerical simulations of single bubble cavitation events.^{40–42} Storey and Szeri⁴¹ (26.5 kHz, 1.2 bar, Ar) calculate that the bubble will be 14% water vapor upon reaching its minimum radius and they predict that H₂O, H \cdot , HO \cdot , and O-atom are the dominate chemical species. Yasui et al.⁴² (300 kHz, 3.0 bar, air) calculate that the bubble will have 10 to 20% water vapor before and after the bubble reaches a minimum size while H \cdot , HO \cdot , and O-atom concentrations range from 0.1 to 1.0% of the bubble contents during temperature maximums. Colussi et al.⁴⁰ (300 kHz, 1.8 atm, Ar) have calculated that HO \cdot , H \cdot , and O-atom concentrations are dissimilar during bubble radius minima at 1.0, 0.1, and 0.01% of the total bubble gas content, respectively.

The [CO]/[CO₂] product ratios for PFOS and PFOA sonolysis are estimated in three cases using relative C₁ fluoro-radical and their secondary C₁ intermediate branching ratios at various concentrations of H₂O, H \cdot , HO \cdot , and O-atom as shown in Table 5. In the first case, H \cdot , HO \cdot , and O-atom concentrations are all set to 1%, in the second case H \cdot , HO \cdot , and O-atom are set to 0.1% and in the final case HO \cdot , H \cdot , and O-atom are set to 1.0, 0.1, and 0.01%, respectively. For all three cases, vapor concentrations were set at 10%, 1.0% or 0.1%. The primary transformation pathways (i.e., those with branching ratios >0.01) are shown in Scheme 3 with the primary reactant listed above the reaction arrow.

In Table 5 are the bubble vapor conditions used for the estimations, the CO/CO₂ branching ratios for the secondary C₁ intermediates, the PFOS and PFOA estimated CO/CO₂ branching ratios and the estimated branching ratio over the experimentally determined branching ratio. The bubble vapor conditions that result in a best fit to the experimental data were 10% water vapor and 1% or 0.1% H \cdot , HO \cdot , and O-atom. When the range of radical concentrations was varied, the CO/CO₂ branching ratios were underestimated by 55–80%. This underestima-

SCHEME 3: Detailed Representation of Possible C₁ Fluoro-Radical Transformation Pathways that May Occur in the Transiently Cavitating Bubble Vapor (Step 5, Scheme 1)^a

^a The initial C₁ fluoro-radicals are in boxes and the final products are in ovals. The bimolecular reactant is listed either above the reaction arrow or to the right of vertical reaction arrows. If multiple reactants are listed they signify multiple individual pathways and not sequential reactions.

tion was primarily due to the reduced H \cdot vapor concentration, H \cdot /HO \cdot = 0.1, yielding a more oxidizing bubble vapor and thus the more oxidized carbon product, CO₂. The CO/CO₂ branching ratios for CFO and CF₂O are observed to favor CO₂ over CO upon decreasing H \cdot concentration. Reducing the relative water vapor concentration increases the CO branching ratio of CF₂O.

An analogous calculation as presented above for the unimolecular decomposition of the initial fluorochemical intermediate can be used to estimate the number of acoustic cycles, or sonication time, for the C₁ fluoro-radicals in Scheme 3 to completely pyrolyze into CO and CO₂. If we considered the reaction with the longest half-life, COF₂ + H₂O \rightarrow CO₂ + 2 HF, at 8.15 μ s (4000 K, 10% H₂O) and that eight half-lives are needed to destroy >99% of the initial compound the time for complete transformation would be 65 μ s. Using a conservative 0.50 ns high-temperature period per cycle, it will take 1.3 \times 10⁵ acoustic cycles to completely eliminate COF₂. Likewise, the total time for the sonolytic transformation of the C₁-fluororadical is estimated to be 0.36 s (2.8 μ s per cycle at 354 kHz). The calculated time is inline with the characteristic degradation time (e.g., 1 to 3 s) using the empirical Henry's constant estimation.⁴⁵ And once again, this calculation is in general agreement with, but much shorter than, the experimentally observed fluoride production half-life of 2 min. The discrepancy between calculation and experiment suggests that fluorochemical intermediates partitioning to the bubble vapor phase and not pyrolytic degradation may be the rate-limiting

step in fluoride production. More importantly, both experimental results and kinetic estimations agree with the conclusion that shortly after the sonochemical decomposition of a perfluorinated surfactant, PFOS or PFOA, their sono-intermediates are transformed relatively quickly into inorganic constituents of PFOX: F^- , SO_4^{2-} , CO , and CO_2 .

Conclusions

Perfluorinated surfactants are widespread in the environment and recalcitrant toward most conventional water treatment technologies. Incineration is a viable method for degradation of concentrated manufacturing wastes, yet not efficient for more dilute aqueous solutions. Acoustic cavitation as driven by ultrasonic cavitation has been shown to be both effective and relatively fast method for the complete destruction and mineralization of PFOS and PFOA over a wide range of initial concentrations. Conventional methods such as hydroxyl radical oxidation¹³ and biodegradation⁸ have been shown to have minimal effect the elimination on these compounds from water. Photodegradation techniques^{15,16,21,22,24,26} as well as elemental iron reduction in subcritical water²⁹ have been shown to degrade these species. However, minimum degradation half-lives are in the range of 45–120 min and achieve a maximum of 50% mineralization with shorter perfluorinated acids produced as byproducts. These latter products are just as recalcitrant as the initial perfluorinated compounds. The PFOS and PFOA degradation rates presented here both have a degradation half-life of 30 min or less and achieve complete mineralization immediately after the decomposition of the initial product as shown by time-dependent product analysis and kinetic estimations. Previous studies⁷³ have shown that sololytic rates can be scaled linearly by increasing acoustic power density and scaling-up the reactor size has minimal effect on the observed reaction rates. Therefore, ultrasonically driven acoustic cavitation provides a technically viable method for the treatment of aqueous perfluorinated surfactant wastewaters over a rather wide range of concentrations, i.e., 10 nM (5 ppb) to 10 mM (5 ppm) in this study.

Acknowledgment. We thank the 3M Company for ongoing research support. This support included the donation to Caltech of analytical standards and an Agilent LC-MS-Ion Trap mass spectrometer. Special thanks are given to Dale Bacon of the 3M Environmental Laboratory for his insight, useful comments, and guidance on this research project. The authors also thank Dr. A.J. Colussi for helpful discussions and Dr. Nathan Dalleska of the Environmental Analytical Center.

Supporting Information Available: Details of the analytical procedures used (PDF). This material is available free of charge via the Internet at <http://pubs.acs.org>.

References and Notes

- (1) 3M Company. *The Science of Organic Fluorochemistry*; docket AR226–0547; Office of Pollution Prevention and Toxics, U.S. Environmental Protection Agency: Washington, D.C., 1999; p 12.
- (2) Sinclair, E.; Kannan, K. *Environ. Sci. Technol.* **2006**, *40*, 1408.
- (3) Schultz, M. M.; Higgins, C. P.; Huset, C. A.; Luthy, R. G.; Barofsky, D. F.; Field, J. A. *Environ. Sci. Technol.* **2006**, *40*, 7350.
- (4) Boulanger, B.; Vargo, J. D.; Schnoor, J. L.; Hornbuckle, K. C. *Environ. Sci. Technol.* **2005**, *39*, 5524.
- (5) Martin, J. W.; Whittle, D. M.; Muir, D. C. G.; Mabury, S. A. *Environ. Sci. Technol.* **2004**, *38*, 5379.
- (6) Martin, J. W.; Smithwick, M. M.; Braune, B. M.; Hoekstra, P. F.; Muir, D. C. G.; Mabury, S. A. *Environ. Sci. Technol.* **2004**, *38*, 373.
- (7) Schultz, M. M.; Barofsky, D. F.; Field, J. A. *Environ. Eng. Sci.* **2003**, *20*, 487.
- (8) Key, B. D.; Howell, R. D.; Criddle, C. S. *Environ. Sci. Technol.* **1998**, *32*, 2283.
- (9) Hollingsworth, J.; Sierra-Alvarez, R.; Zhou, M.; Ogden, K. L.; Field, J. A. *Chemosphere* **2005**, *59*, 1219.
- (10) 3M Company. Docket AR226–0489; Office of Pollution Prevention & Toxics, U.S. Environmental Protection Agency: Washington D.C., 1978; p 19.
- (11) 3M Company. Docket AR226–0058; Office of Pollution Prevention & Toxics, U.S. Environmental Protection Agency: Washington, D.C., 1994; p 4.
- (12) Oppenlander, T. *Photochemical Purification of Water and Air*; Wiley-VCH: Weinheim, Germany, 2003.
- (13) Schroder, H. F.; Meesters, R. J. W. *J. Chromatogr., A* **2005**, *1082*, 110.
- (14) Moriwaki, H.; Takagi, Y.; Tanaka, M.; Tsuruho, K.; Okitsu, K.; Maeda, Y. *Environ. Sci. Technol.* **2005**, *39*, 3388.
- (15) Hori, H.; Hayakawa, E.; Einaga, H.; Kutsuna, S.; Koike, K.; Ibusuki, T.; Kiatagawa, H.; Arakawa, R. *Environ. Sci. Technol.* **2004**, *38*, 6118.
- (16) Chen, J.; Zhang, P. *Water Sci. Technol.* **2006**, *54*.
- (17) 3M Company. Docket AR226–0056; Office of Pollution Prevention & Toxics, U.S. Environmental Protection Agency: Washington DC, 1978; p 17.
- (18) 3M Company. Docket AR226–0490; Office of Pollution Prevention & Toxics, U.S. Environmental Protection Agency: Washington D.C., 1979; p 15.
- (19) Yamamoto, T.; Noma, Y.; Sakai, S. I.; Shibata, Y. *Environ. Sci. Technol.* **2007**, *41*, 5660.
- (20) Chen, J.; Zhang, P. Y.; Liu, J. *J. Environ. Sci.* **2007**, *19*, 387.
- (21) Hori, H.; Yamamoto, A.; Hayakawa, E.; Taniyasu, S.; Yamashita, N.; Kutsuna, S.; Kiatagawa, H.; Arakawa, R. *Environ. Sci. Technol.* **2005**, *39*, 2383.
- (22) Hori, H.; Yamamoto, A.; Kutsuna, S. *Environ. Sci. Technol.* **2005**, *39*, 7692.
- (23) Kutsuna, S.; Hori, H. *Int. J. Chem. Kin.* **2007**, *276*.
- (24) Chen, J.; Zhang, P. Y.; Zhang, L. *Chem. Lett.* **2006**, *35*, 230.
- (25) Hori, H.; Hayakawa, E.; Koike, K.; Einaga, H.; Ibusuki, T. *J. Mol. Catal. A: Chem.* **2004**, *211*, 35.
- (26) Dillert, R.; Bahnemann, D.; Hidaka, H. *Chemosphere* **2007**, *67*.
- (27) Yuan, Q.; Ravikrishna, R.; Valsaraj, K. T. *Sep. Purif. Technol.* **2001**, *24*.
- (28) Hidaka, H.; Jou, H.; Nohara, K.; Zhao, J. *Chemosphere* **1992**, *25*, 1589.
- (29) Hori, H.; Nagaoka, Y.; Yamamoto, A.; Sano, T.; Yamashita, N.; Taniyasu, S.; Kutsuna, S.; Osaka, I.; Arakawa, R. *Environ. Sci. Technol.* **2006**, *40*, 1049.
- (30) Kolaczowski, S. T.; Plucinski, P.; Beltran, F. J.; Rivas, F. J.; McLurgh, D. B. *Chem. Eng. J.* **1999**, *73*, 143.
- (31) Vinodgopal, K.; Ashokkumar, M.; Grieser, F. *J. Phys. Chem. B* **2001**, *105*, 3338.
- (32) Destailats, H.; Hung, H. M.; Hoffmann, M. R. *Environ. Sci. Technol.* **2000**, *34*, 311.
- (33) Hua, I.; Hoffmann, M. R. *Environ. Sci. Technol.* **1996**, *30*, 864.
- (34) Kotronarou, A.; Mills, G.; Hoffmann, M. R. *J. Phys. Chem.* **1991**, *95*, 3630.
- (35) Petrier, C.; David, B.; Laguian, S. *Chemosphere* **1996**, *32*, 1709.
- (36) Brennen, C. E. *Cavitation and Bubble Dynamics*; Oxford University Press: New York, 1995.
- (37) Misik, V.; Miyoshi, N.; Riesz, P. *J. Phys. Chem.* **1995**, *99*, 3605.
- (38) Leighton, T. G. *The Acoustic Bubble*; Academic Press: London, 1994.
- (39) Didenko, Y. T.; McNamara, W. B.; Suslick, K. S. *J. Phys. Chem. A* **1999**, *103*, 10783.
- (40) Colussi, A. J.; Weavers, L. K.; Hoffmann, M. R. *J. Phys. Chem. A* **1998**, *102*, 6927.
- (41) Storey, B. D.; Szeri, A. J. *Proc. R. Soc. London, Ser. A* **2000**, *456*, 1685.
- (42) Yasui, K.; Tuziuti, T.; Kozuka, T.; Towata, A.; Iida, Y. *J. Chem. Phys.* **2007**, *127*.
- (43) Krishna, C. M.; Lion, Y.; Kondo, T.; Riesz, P. *J. Phys. Chem.* **1987**, *91*, 5847.
- (44) Jennings, B. H.; Townsend, S. N. *J. Phys. Chem.* **1961**, *65*, 1574.
- (45) Colussi, A. J.; Hung, H. M.; Hoffmann, M. R. *J. Phys. Chem. A* **1999**, *103*, 2696.
- (46) Yang, L. M.; Rathman, J. F.; Weavers, L. K. *J. Phys. Chem. B* **2005**, *109*, 16203.
- (47) Sostaric, J. Z.; Riesz, P. *J. Am. Chem. Soc.* **2001**, *123*, 11010.
- (48) Henglein, A.; Kormann, C. *Int. J. Radiat. Biol.* **1985**, *48*, 251.
- (49) Manousaki, E.; Psillakis, E.; Kalogerakis, N.; Mantzavinos, D. *Water Res.* **2004**, *38*, 3751.
- (50) Glockner, V.; Lunkwitz, K.; Prescher, D. *Tenside, Surfactants, Deterg.* **1989**, *26*.
- (51) Krusic, P. J.; Marchione, A. A.; Roe, D. C. *J. Fluorine Chem.* **2005**, *126*, 1510.

- (52) Lazerte, J. D.; Hals, L. J.; Reid, T. S.; Smith, G. H. *J. Am. Chem. Soc.* **1953**, *75*, 4525.
- (53) Ainagos, A. F. *Kinet. Catal.* **1991**, *32*, 720.
- (54) Harada, H. *Ultrason. Sonochem.* **1998**, *5*, 73.
- (55) Henglein, A. Z. *Naturforsch., B: Chem. Sci.* **1985**, *40*, 100.
- (56) Lopez-Fontan, J. L.; Gonzalez-Perez, A.; Costa, J.; Ruso, J. M.; Prieto, G.; Schulz, P. C.; Sarmiento, M. *J. Colloid Interface Sci.* **2006**, *294*, 458.
- (57) Lopez-Fontan, J. L.; Sarmiento, F.; Schulz, P. C. *Colloid Polym. Sci.* **2005**, *283*, 862.
- (58) Simister, E. A.; Lee, E. M.; Lu, J. R.; Thomas, R. K.; Ottewill, R. H.; Rennie, A. R.; Penfold, J. *J. Chem. Soc., Faraday Trans.* **1992**, *88*, 3033.
- (59) Shinoda, K.; Hato, M.; Hayashi, T. *J. Phys. Chem.* **1972**, *76*, 909.
- (60) Lesko, T.; Colussi, A. J.; Hoffmann, M. R. *Environ. Sci. Technol.* **2006**, *40*, 6818.
- (61) Lines, D.; Sutcliffe, H. *J. Fluorine Chem.* **1984**, *25*, 505.
- (62) Krusic, P. J.; Roe, D. C. *Anal. Chem.* **2004**, *76*, 3800.
- (63) Hung, H. M.; Hoffmann, M. R. *Environ. Sci. Technol.* **1998**, *32*, 3011.
- (64) Hung, H. M.; Hoffmann, M. R. *J. Phys. Chem. A* **1999**, *103*, 2734.
- (65) Goss, K. U.; Bronner, G. *J. Phys. Chem. A* **2006**, *110*, 9518.
- (66) Goss, K. U.; Bronner, G.; Harner, T.; Monika, H.; Schmidt, T. C. *Environ. Sci. Technol.* **2006**, *40*, 3572.
- (67) Goss, K.-U. *Environ. Sci. Technol.* **2008**, *42*, 456.
- (68) Kato, S.; Makide, Y.; Tominaga, T.; Takeuchi, K. *J. Phys. Chem.* **1987**, *91*, 4278.
- (69) Longfellow, C. A.; Berrie, C. L.; Suits, A. G.; Lee, Y. T. *J. Chem. Phys.* **1997**, *107*, 7202.
- (70) Ciawi, E.; Rae, J.; Ashokkumar, M.; Grieser, F. *J. Phys. Chem. B* **2006**, *110*, 13656.
- (71) Didenko, Y. T.; McNamara, W. B.; Suslick, K. S. *J. Am. Chem. Soc.* **1999**, *121*, 5817.
- (72) Burgess, D. R.; Zachariah, M. R.; Tsang, W.; Westmoreland, P. R. *Prog. Energy Combust. Sci.* **1995**, *21*, 453.
- (73) Destailats, H.; Lesko, T. M.; Knowlton, M.; Wallace, H.; Hoffmann, M. R. *Ind. Eng. Chem. Res.* **2001**, *40*, 3855.
- (74) Galyautdinov, I. V.; Nazmeeva, S. R.; Savchenko, R. G.; Ves'kina, N. A.; Nedopekin, D. V.; Fatykhov, A. A.; Khalilov, L. M.; Odinkov, V. N. *Russ. J. Org. Chem.* **2004**, *40*, 675.
- (75) Huang, B. N.; Haas, A.; Lieb, M. *J. Fluorine Chem.* **1987**, *36*, 49.
- (76) Mackay, D.; Bobra, A.; Chan, D. W.; Shiu, W. Y. *Environ. Sci. Technol.* **1982**, *16*, 645.
- (77) Schwarzenbach, R. P.; Gschwend, P. M.; Imboden, D. M. *Environmental Organic Chemistry*, 2nd ed.; Wiley: New York, 2003.
- (78) Maruthamuthu, P.; Padmaja, S.; Huie, R. E. *Int. J. Chem. Kinet.* **1995**, *27*.
- (79) Mashino, M.; Ninomiya, Y.; Kawasaki, M.; Wallington, T. J.; Hurley, M. D. *J. Phys. Chem. A* **2000**, *104*, 7255.
- (80) Yamamoto, O.; Takahashi, K.; Inomata, T. *J. Phys. Chem. A* **2004**, *108*, 1417.
- (81) Hine, J.; Mookerjee, P. K. *J. Org. Chem.* **1975**, *40*, 292.